Host-derived CEACAM-laden vesicles engage enterotoxigenic *E. coli* for elimination and toxin neutralization.

Alaullah Sheikh[1], Debayan Ganguli[1], Tim J. Vickers[1], Bernhard Singer[2*], Jennifer Foulke-Abel[3], Marjahan Akhtar[1,4], Nazia Khatoon[1], Bipul Setu[1], Supratim Basu[1], Clayton Harro[5*], Nicole Maier[6], Wandy L. Beatty[7], Subhra Chakraborty[5], Tafiqur R. Bhuiyan[4], Firdausi Qadri[4], Mark Donowitz[3], and James M. Fleckenstein[1,8]

[1]Division of Infectious Diseases, Department of Medicine, Washington University in Saint Louis, School of Medicine, Saint Louis, Missouri, USA; [2]Institute of Anatomy, Medical Faculty, University of Suisberg-Essen, 45147 Essen, Germany; [3]Division of Gastroenterology & Hepatology, Johns Hopkins University School of Medicine, Baltimore, Maryland, USA; [4]International Centre for Diarrhoeal Disease Research, Bangladesh; Dhaka, Bangladesh. [5]Department of International Health, Division of Global Disease Epidemiology and Control, Johns Hopkins Bloomberg School of Public Health; [6]PATH, Seattle Washington, USA; Department of Molecular Microbiology, Washington University School of Medicine, Saint Louis, Missouri, USA; [8]Medicine Service, Infectious Disease Section, Veterans Affairs Health Care System, Saint Louis, Missouri, USA.

corresponding author
James M. Fleckenstein
Division of Infectious Diseases
Department of Medicine
Washington University School of Medicine
Campus Box 8051
660 South Euclid Avenue
Saint Louis Missouri, USA 63110
p 314-362-9218
jfleckenstein@wustl.edu

*deceased

Keywords

enterotoxigenic *Escherichia coli* (ETEC); cell adhesion molecules; diarrhea; host- pathogen interactions; extracellular vesicles.

abstract

Enterotoxigenic *Escherichia coli* (ETEC) cause hundreds of millions of diarrheal illnesses annually ranging from mildly symptomatic cases to severe, life-threatening cholera-like diarrhea. Although ETEC are associated with long-term sequelae including malnutrition, the acute diarrheal illness is largely self-limited. Recent studies indicate that in addition to causing diarrhea, the ETEC heat-labile toxin (LT) modulates the expression of many genes in intestinal epithelia, including carcinoembryonic cell adhesion molecules (CEACAMs) which ETEC exploit as receptors, enabling toxin delivery. Here however, we demonstrate that LT also enhances the expression of CEACAMs on extracellular vesicles (EV) shed by intestinal epithelia and that CEACAM-laden EV increase in abundance during human infections, mitigate pathogen-host interactions, scavenge free ETEC toxins, and accelerate ETEC clearance from the gastrointestinal tract. Collectively, these findings indicate that CEACAMs play a multifaceted role in ETEC pathogen-host interactions, transiently favoring the pathogen, but ultimately contributing to innate responses that extinguish these common infections.

Significance statement

Enterotoxigenic *E. coli,* characterized by the production of heat-labile (LT) and heat-stable (ST) toxins, are a very common cause of diarrhea in low-income regions responsible for hundreds of millions of infections each year, and the major cause of diarrhea in travelers to endemic areas. Although these infections may be severe and cholera-like, they are typically self-limited. These studies demonstrate that extracellular vesicles produced by host intestinal cells can capture the bacteria and its secreted toxins at a distance from the cell surface, potentially acting as molecular decoys to neutralize the enterotoxins and extinguish the infection.

Introduction

Enterotoxigenic *Escherichia coli* (ETEC) comprise a diverse diarrheagenic pathovar defined by the production of heat-labile (LT) and/or heat-stable (ST) enterotoxins. These pathogens are thought to account for hundreds of millions of cases of diarrheal illness annually with young children in low-middle income countries disproportionately affected[1]. ETEC have remained a leading cause of death due to acute diarrheal illness[2], and are associated with long-term sequelae including malnutrition, growth stunting[3,4] and cognitive impairment[5].

The basic mechanism by which these pathogens cause diarrheal illness is well-established. Heat-labile toxin (LT) binds to gangliosides on the intestinal surface, and once internalized stimulates production of cAMP. Heat-stable toxins (ST) bind to guanylate cyclase C on the surface of enterocytes to stimulate production of cGMP. These cyclic nucleotides, cAMP and cGMP, in turn activate protein kinase A (PKA) and protein kinase G (PKG), respectively. Kinase -mediated phosphorylation of cellular ion channels including the cystic fibrosis transmembrane regulator (CFTR), and the sodium hydrogen exchanger (NHE3) modulates ion transport resulting in the net export of NaCl and water into the intestinal lumen leading to watery diarrhea[6].

Diarrheal illness caused by ETEC can range from mild to severe and cholera-like. Indeed, ETEC were initially discovered in patients with *Vibrio cholerae*-negative clinical cholera, and severe ETEC is clinically indistinguishable from cholera[7-11]. Importantly, while ETEC infections can occasionally cause more protracted symptoms[12], acute diarrhea caused by these

77 pathogens is typically self-limited, with resolution after several days. However, what dictates
78 the self-limited nature of ETEC diarrhea is unknown.

79 To cause diarrhea, ETEC must transit to the small intestine, migrate through intestinal
80 mucin[13], and directly engage the brush border of enterocytes to effectively deliver toxin
81 directly at the epithelial surface[14]. ETEC employ both plasmid-encoded adhesins unique to
82 the ETEC pathovar[15] as well as highly conserved chromosomally-encoded type 1 fimbriae to
83 engage enterocytes[16].

84 Recent studies demonstrate that ETEC use type 1 fimbriae[16] to bind to members of a
85 family of extracellular glycoproteins known as carcinoembryonic antigen related cell
86 adhesion molecules (CEACAMs) on the surface of enterocytes, and that these interactions
87 play a critical role in bacterial adhesion and toxin delivery to small intestinal epithelia[17].
88 Moreover, we found that heat-labile toxin accelerates production of CEACAMs by small
89 intestinal enterocytes[17], effectively modifying the epithelial landscape to transiently benefit
90 the pathogen.

91 Notably however, CEACAMs are normally present in abundance in human stool[18 19], with
92 approximately 50-70 mg of carcinoembryonic antigen shed in the course of a day[19]. The
93 majority of fecal CEACAMs are membrane-bound[19], and can be released in soluble form with
94 phosphatidylinositol specific phospholipase C (PI-PLC).

95 Our current studies suggest that CEACAMs play opposing roles in ETEC interactions with
96 gastrointestinal epithelia. While initial expression of these molecules on enterocytes
97 facilitates ETEC-host cell engagement and toxin delivery[17], we demonstrate here that the host
98 may interrupt these encounters by deploying CEACAM-laden extracellular vesicles as decoys

to mitigate effective attachment of the bacteria to the epithelial surface while absorbing and neutralizing secreted ETEC enterotoxins, potentially explaining the self-limited nature of these common infections.

Results

CEACAM expression alters kinetics of ETEC intestinal colonization.

Carcinoembryonic cell adhesion molecules (CEACAMs) are host cell glycoproteins comprising a large subgroup of the immunoglobulin superfamily that form homodimeric intercellular adhesion complexes[20] and which participate in intracellular signaling pathways that can direct cellular differentiation[21]. CEACAMs differ significantly between mice and humans. Although mice have at least 20 putative CEACAM genes, only CEACAM1, CEACAM16, CEACAM18, CEACAM19, and CEACAM20 are shared with humans[22], and all of the GPI-anchored gastrointestinal CEACAM molecules, CEACAMs 5,6, and 7, as well as CEACAM3 which is predominantly on neutrophils, are absent in conventional mice. Therefore, we challenged CEABAC10 transgenic mice[23], which express human CEACAMs 5-7 in the intestine, as well as CEACAM3 to examine the impact on ETEC-host interactions. These studies demonstrated that while gastrointestinal CEACAM expression was associated with modest increases in intestinal colonization immediately after ETEC (jf876, supplemental table 1) challenge (figure 1A, supplemental figure 1A), CEABAC10 mice consistently cleared ETEC more rapidly (figure 1B) than parental C57BL/6NCrl controls suggesting that these molecules play a complex role in directing the kinetics of intestinal colonization.

Examination of intestinal tissues of CEABAC10 transgenic mice revealed that while CEACAMs were expressed on small intestinal mucosal surfaces (figure 2A), we also found many clusters of CEACAM-positive material in the intestinal lumen, (figure 2B-C), Many of the smaller CEACAM-positive structures in the intestinal lumen were in direct contact with the bacteria (inset, figure 2C), suggesting that they may engage ETEC at a distance from the mucosal surface, potentially preventing direct interaction with epithelia. Although CEABAC10 mice may express CEACAM3 on neutrophils[23], we were unable to demonstrate neutrophilic infiltration beyond the basolateral surface of the intestines of infected mice (supplemental figure 1B). Many of the smaller structures ~ 100-300 nm in diameter in the lumen were similar in size to plasma-membrane derived extracellular vesicles (EV)[24,25]. Indeed, we were able to identify multiple individual CEACAM-laden EV (figure 2D), as well as clusters of vesicles (figure 2E), and direct interaction of these EV with bacteria in samples from the ileal lumen of H10407-challenged CEABAC10 mice (figure 2F). Examination of fecal material likewise revealed abundant CEACAM+ EV (figure 2G). Following challenge of CEACAM-expressing mice with ETEC expressing green fluorescent protein (GFP) (jf2450, supplemental table 1), we observed that while individual bacteria shed in stool appeared to be positive for CEACAMs (figure 2H), and we identified CEACAM+ EV bound to ETEC by immunogold transmission electron microscopy of fecal material following challenge (supplemental figure 2), the majority of ETEC emerged in large clusters of bacteria embedded in a CEACAM matrix (figure 2I), (supplemental movie 1).

CEACAMs serve as ETEC decoys and enterotoxin scavengers

Interestingly, while our earlier studies demonstrated that CEACAM6 could be identified on the microvillus surface of enterocytes where it served as a receptor for ETEC[17], transmission electron micrographs of ETEC-infected ileal enteroid monolayers demonstrated large clusters of CEACAM-positive extracellular vesicles (EVs) interposed between the bacteria and microvilli of the intestinal brush border (figure 3A,B). CEACAM6-positive concentrated culture supernatants from polarized human ileal monolayers significantly blocked ETEC adhesion to target intestinal cells, while subtractive absorption with anti-CEACAM antibody partially restored effective adhesion of wild type ETEC to target intestinal epithelial cells further suggesting that CEACAMs can modulate ETEC-host interactions (figure 3C). To determine whether EV could specifically interrupt effective interaction of ETEC with target receptors on enterocytes, we first purified EVs from supernatants of small intestinal enteroid monolayers by size exclusion chromatography (supplemental figure 3a-b), and confirmed the presence of CEACAMs by immunogold labeling (supplemental figure 3c). These CEACAM+ purified vesicles adhered to the surface of ETEC (supplemental figure 4A). Interestingly, while earlier studies suggested that EV, from rat small intestine, impaired the growth of both commensal *E. coli* as well as another *E. coli* pathovar (EPEC) [26], EV isolated from polarized human small intestinal epithelial enteroids had no apparent impact on ETEC growth or survival (supplemental figure 4B,C). However, exogenous administration of these EVs significantly impaired the ability of ETEC to bind to intestinal epithelial cells (figure 3d). We had previously shown that LT increases CEACAM6 expression on the surface of intestinal enterocytes[17]. Notably, CEACAM6 abundance in EV also increased following exposure to LT

and we found that EV obtained from LT-treated ileal monolayers were significantly more effective in blocking ETEC interaction with epithelial cells (figure 3E). Similarly, EV isolated from CEACAM-expressing mice were more effective in preventing bacterial adhesion compared to those from control mice (figure 3F).

We also found that purified EV can bind to heat-labile toxin (figure 4A-C, supplemental figure 5A), and were able to block LT-mediated activation of cAMP in target intestinal cells (figure 4D) suggesting that EV also bear GM1 ganglioside receptors for the LT-B subunit. Indeed, EV effectively competed with target epithelial cells resulting in complete abrogation of toxin delivery to target intestinal epithelia by wild type ETEC (figure 4E). Notably, analysis of CEACAM6+ EV fractions from size exclusion chromatography (SEC) revealed that these EV also bound fluorescently labeled cholera toxin B subunit (CT-B) (supplemental figure 5A), which like LT binds to GM-1 gangliosides. ETEC outer membrane vesicles (OMV) are known to have significant amounts of LT[27,28] which can deliver toxin to host cells[29]. While we demonstrated that purified ETEC OMV could bind directly to GM-1 gangliosides (supplemental figure 5B), we were unable to demonstrate substantial interaction between OMV and EV (supplemental figure 5c), and EV were ineffective in mitigating OMV-directed toxin delivery (supplemental figure 5D), suggesting that EV act primarily by engaging ETEC and free toxin.

In addition, we found that these same EV fractions also possessed guanylate cyclase C (GC-C), the receptor for heat-stable toxins (supplemental figure 5A). By size exclusion chromatography, we demonstrated that glutathione S transferase fused to STh (GST-STh) co-eluted with EV fractions containing CEACAMs (figure 4F, G), and that preincubation of the

GST-STh fusion with EV impaired ST binding to target T84 cells (figure 4H), ultimately leading to significant reduction in toxin-mediated activation of cGMP (figure 4I). In summary these studies suggest that CEACAM-laden EV can engage ETEC and absorb both LT and ST effectively mitigating pathogen-host interactions by serving as molecular decoys for the bacteria as well as its secreted toxins.

heat-labile toxin alters the composition of EVs

Although LT-mediated increases in cAMP, and subsequent activation of PKA are central to acute diarrhea caused by ETEC, PKA also governs the transcription of multiple host genes as it enters the nucleus to phosphorylate the cAMP-response element binding protein CREB[30,31]. Recent studies have demonstrated that LT modulates the transcription of multiple host genes in small intestinal epithelia [17 13 32]. To determine how the composition of EVs might be altered by LT we performed tandem mass spectrometry on vesicles isolated from 2D small intestinal enteroid monolayers with and without LT treatment (supplemental dataset 1). Interestingly, these studies also showed that the abundance of multiple proteins including both CEACAM6 and MUC2 were increased in abundance in EVs from LT-treated enteroids relative to those from controls (Figure 5, supplemental table 3). While the protein with the most increased abundance in LT-treated samples, FCGBP, which like MUC2 is also secreted by goblet cells, and intimately associated with mucin, its actual function remains undetermined[33,34].

We previously observed[32] modulation of proteins linked to brush border biogenesis including the membrane adapter protein BAIAP2L1 involved in microvillus elongation[35,36], or associated with exosomes including CD59 a membrane-bound complement regulatory

protein[37,38]. Notably, our recent transcriptome studies of ileal enteroids also demonstrated that transcription of *myo1a*, a gene encoding microvillar motor protein [26,39] involved in EV biogenesis, is significantly depressed in following exposure to LT, leading us to question whether the quantity of EVs produced by epithelial cells would be impacted by LT exposure. However, short-term exposure (24 h) of small intestinal epithelia to LT had little appreciable impact on either the apparent size or quantity of EVs (supplemental figure 6A). Some suppression of EV production was observed with longer exposures to LT (72 h, supplemental figure 6B). Altogether however, toxin exposure appears to primarily drive changes in EV composition rather than the kinetics of EV biogenesis *in vitro*.

ETEC infection enhances fecal shedding of CEACAMs

In CEACAM-expressing transgenic mice we observed increases in CEACAM shedding in feces following ETEC infection (supplemental figure 7). Examination of stools from children with ETEC diarrheal illness in Bangladesh demonstrated the presence of EV bearing the canonical EV marker CD9 and abundant CEACAMs (figure 6A). As previous immunohistochemistry studies of small intestinal biopsies obtained from ETEC-infected patients demonstrated that CEACAM6 production in the mucosa appeared to increase following infection[17], and earlier studies also showed that CEA (CEACAM 5) is normally shed in significant amounts in human stool[18,19,40,41], we questioned whether the shedding of CEACAMs also increased during human infection. To address this question, we developed a sandwich assay to capture CEACAM-laden material from fecal suspensions of ETEC-infected human hosts (figure 6B). We found that Bangladeshi patients with ETEC had appreciably

higher amounts of CEACAMs in stool compared to healthy controls from the same endemic region(figure 6C), and that on challenge of human volunteers with ETEC, CEACAM content in stool transiently increases in the week following infection (figure 6D), further suggesting that expression of these molecules may play an important role in the innate response to ETEC infection in humans.

Discussion

Enterotoxigenic *E. coli* that cause infections in humans are largely host-restricted pathogens. Recently, we have demonstrated that ETEC engage gastrointestinal CEACAMs, in particular CEACAM6, to facilitate bacterial adhesion and toxin delivery to human intestinal epithelia[17]. Interestingly, the GPI-anchored CEACAMs including CEACAM6 are found exclusively in primates [42], potentially contributing to the unique relationship of ETEC to its human hosts. Indeed, CEACAM molecules appear to be at the center of an evolutionary "arms race" between pathogens and their human hosts. On the one hand, a diverse group of pathogens have evolved a variety of adhesins to engage these molecules as receptors. In contrast, under selective pressure of these pathogens, the host may deploy divergent or variant CEACAMs[43] to minimize adhesin engagement and mitigate host tropism, or to target pathogens for destruction[43-46].

The data presented here suggest a complex paradigm in which the same CEACAM is involved in bacterial adhesion and in innate host defenses. We previously demonstrated that the heat-labile toxin enhances bacterial adhesion by up-regulating target CEACAM6 on the surface of small intestinal enterocytes[17]. Here however, we show that LT also significantly increases CEACAM6 abundance in extracellular vesicles (EV) which can bind the bacteria at a distance to interdict effective adhesion to target enterocytes. Therefore, use of CEACAMs as receptors may ultimately come at some cost to the pathogen as they are eliminated by extracellular CEACAM-laden vesicles.

Notably, these EV also contain GM1 gangliosides, the established receptor for the B-subunits of both LT and the closely related cholera toxin, which like LT also upregulates

254 production of CEACAMs on small intestinal epithelia[17]. Likewise, they bear GC-C, the
255 receptor for heat-stable toxin (ST) as well as the endogenous peptides guanylin and
256 uroguanylin. Notably, the affinity of ST for GC-C is 100 x that of guanylin and 10 x higher than
257 uroguanylin, and both native peptides, unlike ST are subject to proteolysis[47]. Therefore, EV
258 could aid in restoration of intestinal homeostasis by capturing the ST super agonist at a
259 distance from receptors on the surface of epithelial cells, thereby eliminating competition
260 with the lower affinity locally produced endogenous peptides. The ability to engage
261 gastrointestinal pathogen(s) while effectively scavenging any secreted exotoxins may make
262 EV a particularly effective element of innate intestinal defenses.

263 We found that other molecules potentially important in pathogen engagement were also
264 concentrated in CEACAM-positive EVs. The Fc Gamma binding protein (FCGBP) most
265 increased in abundance in EVs from LT treated enteroids, has previously been shown to be
266 associated with exosomes[48,49], and it has been suggested that these mucin-like molecules,
267 which are concentrated in the intestinal goblet cells[50,51], may play an important role in
268 defense of the intestinal mucosa[52,53]. Similarly two other proteins shown here to be
269 enhanced in EVs, CEACAM1 and CLCA1 are also associated with the mucin proteome[54-56],
270 findings that may relate to LT acting as a potent stimulus for goblet cell mucin production and
271 secretion[57].

272 The precise role of EV and the contribution of CEACAMs localized on their surface in the
273 elimination of ETEC and other enteric pathogens deserves additional study. We should also
274 note that in addition to the CEACAMs expressed on mucosal epithelia of the gastrointestinal
275 tract, CEABAC10 mice also express low levels of CEACAM3 on neutrophils[23]. Studies of

children with ETEC diarrhea have demonstrated significant amounts of lactoferrin as well as the leukocytes in stool[58]. In addition, single nucleotide polymorphisms in the lactoferrin gene have been associated with an increased risk of traveler's diarrhea[59], suggesting a role for recruitment of neutrophils in innate responses to ETEC infection. Although CEACAM6 and CEACAM3 share similar amino-terminal IgV-like domains[21], our earlier studies suggested that ETEC preferentially engage CEACAM6 with little or no affinity for CEACAM3[17]. Overall, the current studies demonstrate that ETEC encounter CEACAM-laden vesicles *en route* to target intestinal epithelial cells, and that these have the potential to modulate the course of infection. The significant differences observed in the kinetics of infection between wild type and CEACAM-expressing transgenic mice may also point out limitations to the use of conventional mice in the investigation of ETEC and other *E. coli* pathovars.

Altogether, CEACAMs appear to play a bifunctional role in the pathogenesis of ETEC, acting both as toxin-induced receptors for these common pathogens as well as toxin-responsive molecular decoys for their elimination. These findings have important implications for the investigation of the molecular pathogenesis of ETEC and other gastrointestinal pathogens.

Materials and Methods

propagation of human small intestinal enteroids and transformed intestinal cells

Enteroids from human small intestine were propagated as previously described[17]. Briefly, cells originated from biopsy samples obtained from adults undergoing routine endoscopy with their consent and approval of the Washington University in Saint Louis School of Medicine Institutional Review Board. Stem cells derived from these samples were maintained in a biobank of the Precision Animal Models and Organoids Core (PAMOC) of the Washington University in Saint Louis Digestive Diseases Research Core Center (DDRCC). Samples from human ileum (Hu235D) were re-suspended in Matrigel (BD Bisosciences, San Jose, California, USA), incubated at 37° C and 5% CO_2 with 50% L-WRN conditioned media (CM) and 50% primary culture medium (Advanced DMEM/F12, Invitrogen) supplemented with 20% FBS, 2mM L-glutamine, 100 units/mL penicillin, 0.1mg/mL streptomycin, 10 µM Y-27632 (ROCK inhibitor, Tocris Bioscience, R&D systems, Minneapolis, MN, USA), and 10 µM SB431541 (TGFBR1 inhibitor, Tocris Bioscience, R&D systems).

After washing and trypsinization cells were centrifuged (1100 x g for 5 minutes), then re-suspended (1:1 CM and primary medium with Y-27632 and SB431541) as described above, and plated onto filters (Transwells®, 6.5 mm insert, 24 well plate, 0.4 µm polyester membrane, Corning Incorporated, Kennebunk, ME, USA) coated with collagen IV (Millipore Sigma). Inserts were rinsed with DMEM/F12 with HEPES, 10% FBS, L-glutamine, penicillin, and streptomycin, and cells grown to confluency in 50% conditioned media (CM). To

differentiate monolayers media was changed to 5% CM in primary medium + ROCK inhibitor for 48 hours.

Caco-2 cells (ATCC HTB-37) were propagated at 37°C, in an atmosphere of 5% CO_2, in Eagel's Minimum Essential Media (MEM) supplemented with fetal bovine serum (FBS) to a final concentration of 20%. Cells were seeded and grown to confluence in 96 well plates for adhesion assays to determine bacterial adhesion by detergent lysis, or alternatively onto Transwell filters for confocal microscopy. T84 cells (ATCC CCL-248) were propagated in DMEM: F12 Media containing 5 % FBS.

tandem mass tag-mass spectrometry (TMT-MS) of EVs

Sample proteolysis, isobaric mass tag labeling, peptide fractionation, and liquid chromatography-mass spectrometry of EVs isolated from small intestinal enteroids was conducted by the Mass Spectrometry & Proteomics Core, Johns Hopkins University School of Medicine. Samples were reduced, alkylated, and bound to SP3 beads for digestion with 25 µg/mL trypsin (Pierce, MSMS grade) in 100 mM triethylammonium bicarbonate (TEAB) for 16 h at 37 °C. Bead-bound peptides were then labeled in 100 mM TEAB with TMT Pro 16plex Isobaric Mass Tags (Pierce ThermoFisher). Peptides were fractionated by basic reverse phase chromatography and then analyzed on a nano-LC-Orbitrap-Lumos-ETD (ThermoFisher) interfaced with an EasyLC1000 series reverse-phase chromatography. Survey scans (full mass spectrum) were acquired within 375-1600 Da m/z using a Data Dependent Top 15 method with dynamic exclusion of 15 s. MS/MS spectra were searched with Mascot v.2.8.0 against the RefSeq2021_204_Human database. Search qualifiers included trypsin sites with missed

cleavage 2 tolerance, precursor mass tolerance of 5 ppm, and fragment mass tolerance of 0.01 Da. Carbamidomethylation on Cys, TMT 16pro tag on N-terminus, and TMT 16pro tag on Lys were included as fixed peptide modifications. Oxidation on Met and deamidation of Asn and Gln were included as variable modifications. Peptide identifications from the Mascot searches were processed within Proteome Discoverer and Percolator to identify peptides with a confidence threshold of 1% False Discovery Rate, based on an auto-concatenated decoy database search, and to calculate the protein and peptide ratios. Only unique peptides were used for normalization and ratio calculations.

CEACAM expressing transgenic mice

Transgenic mice which express multiple human CEACAM molecules (CEACAMs 3, 5, 6 and 7) were propagated from 2 female heterozygous CEABAC10 mice[23] kindly supplied by the Gray-Owen laboratory at the University of Toronto. These were mated in the Washington University Mouse Genetics Core facility with C57BL/6N Crl (Charles River Laboratories) males. Pups generated from matings were genotyped to identify CEACAM+ heterozygotes. Genotyping was performed on genomic mouse DNA extracted in hot sodium hydroxide/tris (HotSHOT)[60]. Briefly, 1-2 mm tail snips were dissolved in 75 µl of alkaline lysis buffer (25 mM NaOH, 0.2 mM disodium EDTA, pH 12) at 95°C for 30 minutes and then neutralized with equal volume of 40 mM Tris-HCl, pH 5. Presence or absence of the CEACAM5 gene was detected using primers- GACACAGCAAGCTACAAATGTGAAACCCAG (forward) and GCCACAGGTGATATTGTCAGAGGGAAGTGG (reverse) which amplify a 460bp amplicon.

Both male and female mice were used throughout the studies for both CEABAC10 mice and C57BL/6N Crl controls.

Intestinal challenge with enterotoxigenic *E. coli*

7-8 week-old mice were challenged with ETEC by orogastric lavage as previously described[61]. Briefly, mice were pretreated with streptomycin in drinking water (5 g/l) two days prior to challenge to reduce intestinal colonization with competing microbiota, and then returned to water without antibiotics 1 day prior. Two hours prior to challenge mice were treated with famotidine (1.25 mg in a volume of 125 µl) administered intraperitoneally (IP) to reduce gastric acidity, and fasted until gavage with ~1.5 x 10^4 colony forming units of jf876 (supplemental table 1). Stools were collected daily and fecal suspensions were diluted in PBS and plated onto Luria agar containing kanamycin (25 µg/ml). All studies in mice were conducted under protocol 20-0438 approved by the IACUC at Washington University in Saint Louis, School of Medicine.

EV isolation and characterization

EVs were recovered from antibiotic-free supernatants of differentiated small intestinal enteroids propagated from human ileum (Hu235D). Supernatants were centrifuged at 1048 x g for 10 minutes to pellet debris and then concentrated ~ 14-fold to a final volume of 0.5 ml (Amicon, 30K MWCO) prior to additional processing.

To isolate EVs, concentrated supernatants were separated by size exclusion chromatography (SEC) using resin with a 35 nm pore size (qEVoriginal/35 nm, Izon). The size distribution and quantity of EVs was determined by tunable resistance pulse sensing (TPRS)

(qNano, Izon Ltd., Christchurch, New Zealand). All steps of nanopore optimization and sample measurement followed the guidelines outlined in the qNano Gold User Manual and Izon Control Suite software Custom Planner Tool (Izon). For the analysis, a nanopore NP100 (Pore ID A87921, Izon Ltd.) with an analysis range of 50−330 nm was utilized. The optimization of the nanopore was performed using polystyrene calibration particles (CPC100, Batch ID 20221003, Izon Ltd.) with an average particle diameter of 100 nm and a concentration of 1.8E+13 for calibration purposes. Both the calibration particles and the samples were run under the same conditions, including stretch, pressure, voltage, and baseline current. To eliminate the impact of pore and particle charge on the detected concentration, all samples were analyzed at two pressure points.

Dot-immunoblotting of SEC fractions

2 µl of each fraction was spotted onto nitrocellulose membranes, dried at 37°C for 5 minutes, blocked with 5% milk in PBS, 0.05% Tween-20 for 30 minutes at 37°C, then incubated with primary antibodies against CEACAM6 (9A6), CD9 (C-4), lysozyme, or intestinal alkaline phosphatase diluted 1:1000 in 2.5% milk in PBS, 0.05% Tween-20 for 1 hour at 37°C. After washing 3x in PBS, membranes were incubated with the respective anti-mouse or anti-rabbit HRP-conjugated secondary antibodies (1:1000 dilution in PBS) for 45 minutes at room temperature, washed again in PBS, and developed with Clarity ECL Western blot substrate (Bio-Rad,1705061). To detect binding of the cholera toxin B subunit, fluorophore-conjugated CT-B (ThermoFisher C34775) was incubated with membranes prepared as above at a final concentration of 4 µg/ml in PBS 0.05% Tween-20 for 30 minutes

396 at room temperature, washed 3 x im PBS and imaged on an Azure biosytems c600 molecular
397 imager.
398 To detect CEACAMs in the feces of CEABAC10 mice following ETEC infection, fecal
399 pellets were collected prior to infection, and on days 1 and 9 post infection. 300 µg from
400 each mouse was resuspended in resuspension buffer (PBS-0.5% Tween-20 containing 5 mM
401 sodium azide) by vigorous vortexing and centrifuged at 845 x g for 30 minutes at 4°C.
402 Clarified supernatant (2 µl) was dotted onto nitrocellulose as above and probed with rabbit
403 polyclonal anti-CEA primary antibody (1:1000; Dako, Denmark A0115) and HRP conjugated
404 anti-rabbit secondary antibody (1:1000; Rockland, 611-1322). Blots were visualized by
405 chemiluminescence using Clarity Western ECL substrate (Bio-Rad 1705061) and signal
406 intensities were measured using ImageJ2 v2.14.
407
408 To isolate extracellular vesicles from CEABAC10 transgenic mice and littermate controls,
409 mice were sacrificed, the small intestine excised, and flushed 3 times with 5 ml of PBS
410 supplemented with protease inhibitor (Pierce Protease Inhibitor Mini, Thermo Scientific).
411 Debris was removed from the lavage by centrifugation at 1048 x g for 5 minutes, followed by
412 passage of lavage fluid through a 70 µm filter, and concentration through a 3K MWCO filter
413 (Amicon Ultra-4). EVs were then isolated by size exclusion (qEVoriginal/35 nm, Izon).
414 To isolate extracellular vesicles from human fecal specimens, diarrheal samples from ETEC
415 infected patients (n=5) were pooled together and resuspended in 15 ml PBS supplemented
416 with protease inhibitors (Pierce Protease Inhibitor Mini, ThermoFisher Scientific, A32955),

centrifuged at 4°C at 875 x g, filtered through 70 µm filter and concentrated using a 30 kDa MWCO filter (Amicon Ultra-15, Millipore).

Total protein concentration of each vesicle preparation was assessed using the Qubit Protein Assay Kit (Q33212, ThermoFisher). To ensure complete lysis, vesicle samples were incubated with 0.2% SDS for 10 minutes at 95°C. Samples and standards were then incubated with Qubit working solutions for 15 minutes at room temperature and read with a Qubit Fluorometer 3.0.

In CEACAM depletion experiments, anti-CEA rabbit polyclonal antibodies (supplemental table 2) were immobilized onto protein G Dynabeads (Invitrogen) and incubated with culture supernatant at room temperature for 1 hour. CEACAM-depleted supernatant was then separated from beads by magnetic separation. CEACAM depletion was verified by immunoblotting.

transmission electron microscopy

Transmission electron microscopy (TEM) of small intestinal enteroids infected with ETEC was performed in the Department of Molecular Microbiology Imaging Facility. After gentle washing with PBS, samples were first fixed in a solution of 2% paraformaldehyde/2.5% glutaraldehyde (Ted Pella, Inc., Redding, CA) in 100 mM sodium cacodylate buffer, pH 7.2 for 2 hours at room temperature. Samples were then placed at 4°C overnight, and then washed in sodium cacodylate buffer and postfixed in 2% osmium tetroxide (Ted Pella, Inc) for 1 hour at room temperature. After rinsing in deionized water, samples were dehydrated in ethanol, and embedded in Eponate 12 resin (Ted Pella, Inc.) cut into sections (95 nm) with an

ultramicrotome (Leica Ultracut UCT, Leica Microsystems, Inc., Bannockburn, IL), and stained with uranyl acetate and lead citrate.

To immunolabel vesicles, fractions were absorbed onto glow-discharged formvar/carbon-coated nickle grids (Ted Pella, Inc.) for 10 min followed by negative staining. Grids were then washed with PBS and blocked with 1% FBS for 5 min Grids were subsequently incubated with rabbit anti-CEA (Dako, supplemental table 2) for 30 min. Grids were then incubated with secondary goat anti-rabbit IgG antibody conjugated to 12 nm colloidal gold (Jackson ImmunoResearch Laboratories, Inc. 111-205-144, West Grove PA) for 30 min. Grids were then washed, fixed with 1% glutaraldehyde, and stained with 1% aqueous uranyl acetate (Ted Pella Inc., Redding CA) for 1 min. Excess liquid was gently wicked off and grids were allowed to air dry. Samples were viewed on a JEOL 1200 EX transmission electron microscope (JEOL USA Inc., Peabody, MA) equipped with an AMT 8 megapixel digital camera and AMT Image Capture Engine V602 software (Advanced Microscopy Techniques, Woburn, MA).

Intestinal lavage specimens from CEABAC10 mice challenged with ETEC strain jf876 (serotype O78) (table S1) were processed by SEC as above, and concentrated material was then used to identify EV-coated bacteria by immunogold TEM. Grids were incubated with rabbit anti-O78 antisera (Penn State) followed by anti-rabbit 18 nm gold conjugate (Jackson ImmunoResearch) to identify ETEC and mouse anti-CEACAM6 monoclonal antibody (9A6, Santa Cruz) followed by anti-mouse 12 nm gold conjugate.

Purification of recombinant GST-STh fusion protein

Recombinant glutathione S transferase (GST) and GST-STh fusion proteins were purified as previously described[62]. Briefly bacterial strains jf1364 and jf3265 were grown overnight at 37°C, 225 rpm from frozen glycerol stocks in 2 ml of Luria Broth containing carbenicillin (100 µg/ml), diluted in fresh media and grown to OD600 of ~0.6 then induced with isopropyl-β-d-thiogalactopyranoside (IPTG) for 2 hours. Cell pellets were extracted by sonication 5x in the presence of protease inhibitor (Roche Complete 11697498001). Clarified supernatants were loaded onto 3 ml columns packed with glutathione agarose resin (GoldBio G-250-10), and after washing with PBS, recombinant GST or GST-STh was eluted with buffer containing 100 mM Tris-HCl, pH 8.0 and 10 mM reduced glutathione (MilliporeSigma 70-18-8), then dialyzed vs PBS.

ETEC adhesion-inhibition assays

ETEC strain H10407 (supplementary table 1) was grown from frozen glycerol stocks in LB media at 37°C under static conditions as previously described[16] to enhance expression of type 1 pili. Bacteria were added to Caco-2 cells to achieve a MOI (multiplicity of infection) of ~1:10 and incubated with either CEACAM-enriched concentrated supernatants, CEACAM-depleted supernatant, or PBS as a control. To assess the effects of extracellular vesicles (EV) isolated from culture supernatants, the inoculum was incubated with vesicles for 15 minutes at 37°C prior to infection. Following inoculation, polarized Caco-2 cell monolayers were incubated at 37°C in a humidified tissue culture incubator with 5% CO_2. After incubation for an hour, the cell monolayers were washed three times with gentle shaking (100 rpm on an

orbital shaker for 1 minute per wash) using pre-warmed media to remove any unbound bacteria. Cell monolayers were then lysed with 0.1% Triton X-100 for 5 minutes, and the lysates were plated on LB-agar and grown overnight at 37°C to enumerate colony forming units (CFU). Alternatively, infected monolayers on Transwell filters were fixed with 4% PFA for 30 minutes at 37°C prior to immunofluorescence staining.

Toxin binding

EV immobilized on nitrocellulose membranes, and blocked with 5% milk in PBS containing 0.05% Tween-20, were probed with double mutant heat-labile toxin (dmLT, L192G/L211A) at a concentration of 4 µg/ml to examine binding of LT to EV. LT binding was detected with mouse antisera raised against dmLT[63] (1:1000), followed by horse anti-mouse IgG conjugated to HRP (Cell Signaling 7076, 1:1000), and developed with ECL substrate. Blots were then imaged on an Azure biosytems c600 molecular imager. Alternatively, EV (0.22 mg/ml in a final volume of 100 µl/well) were immobilized on ELISA plates (Costar, 2580) incubation overnight at 4°C. The following day plates were washed and blocked with 5%BSA in PBS for 1 hour at 37°C. After washing with PBS, plates were incubated with increasing concentrations of LT for 1 hour at 37°C. After washing 3x with PBS, bound LT was detected using mouse polyclonal antisera against LT (1:1000, x 1 hour at 37°C), washing 3x with PBS, incubated with HRP-conjugated horse-anti-mouse IgG secondary antibody (Cell Signaling 7076; 1:2000, x 1 hour at 37°C), and developed with 3, 3', 5, 5' - tetramethylbenzidine peroxidase substrate (TMB, sera care 5120-0053). ELISA readings were acquired kinetically and recorded as Vmax (milli-units/min) (Eon, BioTek).

EV-toxin Molecular interaction assays

Purified heat-labile toxin B subunit (LT-B), graciously provided by John D. Clements, Tulane University, was biotinylated (EZ-Link Sulfo-NHS-LC-Biotin) (Thermo Scientific 21335) according to the manufacturer's protocol, and dialyzed to remove excess biotin. Biotinylated LT-B ligand (10 µg) was then added to purified EV (~11 µg) and incubated for 1 hour at 37°C in a final volume of 100 µl. An equal volume of PBS containing biotinylated LT-B was used as a negative control. Protein G magnetic beads (Invitrogen 10003D) were combined with anti-CEA antibody (Dako), and then used to capture EV for 1 hour at room temperature. Following magnetic separation, beads were washed in PBS then incubated in SDS loading dye for 15 minutes at 95°C. Solubilized proteins were resolved by 10% SDS-PAGE, and transferred to nitrocellulose then developed with Avidin-HRP (BioRad 1706528, 1:25,000) followed by enhanced chemiluminescent (ECL) substrate (ThermoFisher Scientific 34094).

Size exclusion chromatography was performed to demonstrate interaction between heat-stable toxin (STh) expressed as a recombinant GST fusion protein and EV. Supernatant media from Hu235D small intestinal enteroids was first concentrated (~7-fold) through a 30 kD MWCO filter (Amicon Ultra-15, Millipore Sigma UFC903024) to a final volume of ~1 ml. 500 µl of concentrate was then incubated for 30 minutes at 37°C with either GST alone or GST-STh. Mixtures were then subjected to size exclusion chromatography (35 nm qEVoriginal, Izon), fractions collected and saved at -80°C for subsequent analysis by dot immunoblotting with antibodies against GST (Invitrogen 13-6700), or anti-CEACAM6 (Santa Cruz 9A6), followed by anti-mouse IgG HRP conjugated antibodies (Cell Signaling 7076S). Fractions 6 to 9 which showed maximum GST and CEACAM6 signals in the dotblot assay were resolved by 10%

SDS-PAGE, and Western immunoblots processed as above and developed with enhanced chemilumincent substrate (ThermoFisher 34094).

Toxin neutralization by EV

To investigate the impact of EV on ETEC toxin delivery target Caco-2 cells (ATCC HTB-37) were seeded in 96 well tissue culture plates at a density of ~3 x 10^4 cells/well, and incubated at 37°C, 5% CO_2 for 48 hours. H10407 was grown under static conditions at 37°C as previously described[16], and ~ 10^6 cfu (Multiplicity of infection~100:1) were added per well with competing EV (~11.5 µg/well) an equal volume of media. Following addition of bacteria ± EV, infected monolayers were incubated at 37°C, 5 % CO_2 for 2 hours, washed to remove excess bacteria, media replaced, and then cellular cAMP was determined by competitive ELISA (Arbor Assays, k019-h). To examine the ability of EV to bind and neutralize LT, 2.5 ng of LT was added to 11.5 µg of purified EV or an equivalent volume of PBS. After incubation for 1 hour at 37°C, the LT ± EV mixtures were added to target Caco-2 cells and incubated for 18 hours at 37°C, 5 % CO_2 prior to determination of cAMP levels as above. For ST neutralization, 1 mg of GST-STh in a volume of 1 ml was reduced with DTT (5 mM) for 3 hours at room temperature. After addition of 2 units of native bovine protein disulfide isomerase (PDI) (Creative Enzymes, NATE-0533), the sample was dialyzed overnight against 1 liter of PBS. Following incubation with EV or buffer control, samples were passed through a 100K MWCO filter (Amicon UFC510008) to retain bound GST-STh. Filtrates were diluted 2 fold in tissue culture media then added to target T84 cells in the presence of phosphodiesterase inhibitors

(25 µM) , incubated for 4 hours at 37°C, 5% CO_2, and intracellular cGMP determined (Arbor Assays K065).

To detect binding of GST-STh to T84 cells, ~ 50,000 cells were added to Transwell filters (Costar 3470) and propagated for 5 days in DMEM/F12 supplemented with 5% FBS. After washing with 3 x with PBS, cells were incubated for 30 minutes at 37°C with 10 ng/ml of GST-STh in PBS ± 50 µl of Hu235D EV (220 µg/ml total protein concentration), then washed 3 x with PBS. After fixation with 4% paraformaldehyde (37°C x 10 minutes, room temperature x 20 minutes), filters were washed with PBS, then incubated with 2% BSA in PBS for 30 minutes at room temperature. GST-STh was detected with GST-cross-absorbed rabbit anti-GST-STh antibodies[62] followed by goat-anti-rabbit IgG AlexaFluor 488 conjugated secondary antibody. Immunofluorescence signals in confocal images were then quantified with NIS-Elements AR software (Nikon 5.11.01).

Confocal microscopy of cell associated bacteria

Cell-associated bacteria were detected using anti-O78 rabbit primary antibody, followed by Alexa Fluor 488 fluorophore conjugated goat anti-rabbit secondary antibody (A11008, ThermoFisher) and imaged by confocal microscopy (Nikon ECLIPSE Ti2). Nuclei were stained with 4′,6-diamidino-2-phenylindole dihydrochloride (DAPI, Sigma). Images were processed using NIS-Elements AR software version 5.11.01,(Nikon).

Myeloperoxidase Immunohistochemistry of ETEC-infected CEABAC10 intestinal tissue

Small intestinal tissue sections cut from formalin-fixed paraffin-embedded blocks were mounted onto glass slides, then deparaffinized with xylene and treated with 3 % H_2O_2 in

562 methanol for 15 minutes. Antigen unmasking was performed using heat retrieval in Diva
563 Decloaker (Biocare Medical DV200MX) in a pressure cooker at 15 PSI and 99°C for 3 minutes.
564 The sections were then blocked with 1% BSA, 10% normal goat serum in PBS. Slides were
565 incubated with anti-MPO antibody (ab20670, Abcam) at a 1:500 dilution overnight at 4°C,
566 washed, and then incubated with VisuCyte Rabbit HRP Polymer (VC003-025, R&D) at 1:4 for 1
567 hour at room temperature. After washing, the slides were developed with DAB (3,3′-
568 diaminobenzidine, Vector SK-4100) as per the manufacturer's protocol, washed, and
569 counterstained with hematoxylin. Brightfield images were obtained with a BZ-X810
570 microscope (Keyence, IL).
571

572 ## Flow cytometry

573 ### Flow cytometry analysis of CEACAM-coated bacteria

574 We infected human CEACAM-expressing CEABAC10+ adult mice with GFP-expressing
575 ETEC. Two days post-infection, fecal pellets were collected. One hundred micrograms (100
576 µg) of fecal pellets were resuspended in 1 ml of PBS and kept on ice for 15 minutes to allow
577 debris to settle. The liquid portion was collected from the top and centrifuged at 3381 x g for
578 5 minutes to pellet down bacteria. To detect CEACAM-coated bacteria, pellets were then
579 stained with anti-CEA primary antibody (DAKO) at a 1:200 dilution for 1 hour on ice, washed
580 three times with PBS, and then incubated with goat anti-rabbit Alexa-Fluor 594-conjugated
581 secondary antibody at a 1:200 dilution for 1 hour. For each sample, a tube without the anti-
582 CEA primary antibody, but with the secondary antibody, was used as an unstained control. All

583 samples were stained with DAPI at a 1:1000 dilution prior to acquisition. Samples were
584 analyzed using FlowJo software (version 10.9.0). GFP+DAPI+ double-positive events were
585 gated for ETEC, from which the amount of CEACAM-positive and CEACAM-negative bacteria
586 was determined based on the corresponding unstained control.

587 **Live-dead staining**

588 To assess the bactericidal activity of membrane vesicles, we conducted live-dead staining
589 followed by flow cytometry analysis. Both log-phase and stationary phase ETEC cultures were
590 grown in the presence or absence of vesicles for 1 hour, 2.5 hours, and 3.5 hours under
591 different conditions (static or shaking) and in different media (LB, cell culture media, or PBS).
592 After the incubation, bacterial samples were pelleted and resuspended in a live-dead
593 staining buffer (PBS supplemented with 1mM EDTA and 0.1% Na-azide, pH 7.4). To each
594 sample, a final concentration of 50 µM propidium iodide and 420 nM thiazole orange dye
595 was added, followed by vortex mixing and a 5-minute incubation at room temperature.
596 Samples were acquired using a BD FACSCalibur and analyzed with FlowJo software.

597 **immunodetection of CEACAMs in stool**

598 Stool specimens obtained from patients at icddr,b during natural ETEC infection, healthy
599 controls, or from earlier ETEC controlled human infection model studies[64] were shipped on
600 dry ice and maintained at -80°C prior to use. ELISA wells (Costar EIA 2580 Corning,
601 Kennebunk, ME, USA) were coated overnight (4°C) with 100 µl/well of CEACAM6-specific
602 monoclonal antibody (9A6) diluted 1:100 in 50 mM carbonate buffer, pH 9.6. Plates were
603 then washed 6 times with 1x PBS (pH 7.4, Corning) containing 0.05% Tween-20 (Sigma), and

604 blocked with 1% BSA in PBS for one hour at 37°C. Stool samples were extracted in PBS-0.5%
605 Tween-20 containing 5 mM sodium azide, and centrifuged at 845 x g for 30 minutes at 4°C.
606 Clarified supernatants were then diluted 1:10 in PBS. 30 µl of each sample was added per
607 well, and incubated at 37°C for one hour, after which plates were washed 6x with PBS-0.05 %
608 Tween. To detect bound CEACAMs 100 µl of polyclonal rabbit anti-CEA antibody (Dako,
609 Denmark A0115) diluted 1:1000 in PBS, 0.5% BSA was added per well and incubated at 37°C
610 x 1 hour. Plates were again washed 6x with PBS-Tween, and then incubated with 100 µl of
611 HRP-conjugated goat IgG anti rabbit IgG (H&L) (Rockland, 611-1322).
612 All human studies were approved by the Institutional Review Board at Washington
613 University in Saint Louis School of Medicine under protocol number 201110126.

614 ## Data sharing

615 Mass spectrometry and original image data are available on Figshare with Digital Object
616 identifiers in supplemental table 4.

617 ## Statistical analyses

618 Mann-Whitney was used to compare two unpaired groups of nonparametric data. Kruskal-
619 Wallis was used in comparison of three or more groups of data with Dunn's multiple
620 comparisons test. The log-rank (Mantel-Cox) test was used in comparison of survival curves.

621 ## acknowledgements

622 JMF was supported by funding from the Department of Veterans Affairs (5I01BX001469-
623 05), and the National Institute of Allergy and Infectious Diseases (NIAID) of the National
624 Institutes of Health (NIH) R01 AI170949, R01 AI089894, and support by the NIH Washington

University DDRCC Grant NIDDK P30 DK052574. Research conducted by AS was also supported by National Institute of Allergy and Infectious Diseases of the National Institutes of Health under Award Number T32AI007172. Mass Spectrometry was conducted in the Proteomics Core of the Johns Hopkins Conte Digestive Diseases Basic and Translational Research Core Center (P30 DK-089502) with the assistance of the Proteomics Core Director, Robert Cole, Ph.D**.** The content is solely the responsibility of the authors and does not necessarily represent the official views of the National Institutes of Health, or the Department of Veterans Affairs.

References

1 Khalil, I. A. *et al.* Morbidity and mortality due to shigella and enterotoxigenic Escherichia coli diarrhoea: the Global Burden of Disease Study 1990-2016. *Lancet Infect Dis* **18**, 1229-1240 (2018). https://doi.org/10.1016/S1473-3099(18)30475-4

2 Kotloff, K. L. *et al.* Burden and aetiology of diarrhoeal disease in infants and young children in developing countries (the Global Enteric Multicenter Study, GEMS): a prospective, case-control study. *Lancet* **382**, 209-222 (2013). https://doi.org/10.1016/S0140-6736(13)60844-2

3 Black, R. E., Brown, K. H. & Becker, S. Effects of diarrhea associated with specific enteropathogens on the growth of children in rural Bangladesh. *Pediatrics* **73**, 799-805 (1984).

4 Nasrin, D. *et al.* Pathogens associated with linear growth faltering in children with diarrhea and impact of antibiotic treatment: The Global Enteric Multicenter Study. *J Infect Dis* (2021). https://doi.org/10.1093/infdis/jiab434

5 Kotloff, K. L. *et al.* The incidence, aetiology, and adverse clinical consequences of less severe diarrhoeal episodes among infants and children residing in low-income and middle-income countries: a 12-month case-control study as a follow-on to the Global Enteric Multicenter Study (GEMS). *Lancet Glob Health* **7**, e568-e584 (2019). https://doi.org/10.1016/S2214-109X(19)30076-2

6 Fleckenstein, J. M. & Sheikh, A. Emerging Themes in the Molecular Pathogenesis of Enterotoxigenic Escherichia coli. *J Infect Dis* (2021). https://doi.org/10.1093/infdis/jiab359

7 Sack, R. B. The discovery of cholera - like enterotoxins produced by Escherichia coli causing secretory diarrhoea in humans. *The Indian journal of medical research* **133**, 171-180 (2011).

8 Carpenter, C. C. *et al.* Clinical and physiological observations during an epidemic outbreak of non-vibrio cholera-like disease in Calcutta. *Bull World Health Organ* **33**, 665-671 (1965).

9 Gorbach, S. L., Banwell, J. G., Chatterjee, B. D., Jacobs, B. & Sack, R. B. Acute undifferentiated human diarrhea in the tropics. I. Alterations in intestinal micrflora. *The Journal of clinical investigation* **50**, 881-889 (1971). https://doi.org/10.1172/JCI106560

10 Sack, R. B. *et al.* Enterotoxigenic Escherichia coli isolated from patients with severe cholera-like disease. *J Infect Dis* **123**, 378-385 (1971).

11 Vicente, A. C. *et al.* Outbreaks of cholera-like diarrhoea caused by enterotoxigenic Escherichia coli in the Brazilian Amazon Rainforest. *Trans R Soc Trop Med Hyg* **99**, 669-674 (2005).

12 Roels, T. H. *et al.* Clinical features of infections due to Escherichia coli producing heat-stable toxin during an outbreak in Wisconsin: a rarely suspected cause of diarrhea in the United States. *Clin Infect Dis* **26**, 898-902 (1998).

13 Sheikh, A. *et al.* Enterotoxigenic Escherichia coli degrades the host MUC2 mucin barrier to facilitate critical pathogen-enterocyte interactions in human small intestine. *Infect Immun*, IAI0057221 (2021). https://doi.org/10.1128/IAI.00572-21

14 Dorsey, F. C., Fischer, J. F. & Fleckenstein, J. M. Directed delivery of heat-labile enterotoxin by enterotoxigenic Escherichia coli. *Cell Microbiol* **8**, 1516-1527 (2006). https://doi.org/10.1111/j.1462-5822.2006.00736.x

15 Roy, K. *et al.* Enterotoxigenic Escherichia coli EtpA mediates adhesion between flagella and host cells. *Nature* **457**, 594-598 (2009). https://doi.org/10.1038/nature07568

16 Sheikh, A. *et al.* Highly conserved type 1 pili promote enterotoxigenic E. coli pathogen-host interactions. *PLoS Negl Trop Dis* **11**, e0005586 (2017). https://doi.org/10.1371/journal.pntd.0005586

17 Sheikh, A. *et al.* CEACAMs serve as toxin-stimulated receptors for enterotoxigenic Escherichia coli. *Proc Natl Acad Sci U S A* **117**, 29055-29062 (2020). https://doi.org/10.1073/pnas.2012480117

18 Kuroki, M., Koga, Y. & Matsuoka, Y. Purification and characterization of carcinoembryonic antigen-related antigens in normal adult feces. *Cancer research* **41**, 713-720 (1981).

19 Matsuoka, Y. *et al.* Characterization of carcinoembryonic antigen-related antigens in normal adult feces. *Jpn J Cancer Res* **81**, 514-519 (1990).

20 Bonsor, D. A., Gunther, S., Beadenkopf, R., Beckett, D. & Sundberg, E. J. Diverse oligomeric states of CEACAM IgV domains. *Proc Natl Acad Sci U S A* **112**, 13561-13566 (2015). https://doi.org/10.1073/pnas.1509511112

21 Gray-Owen, S. D. & Blumberg, R. S. CEACAM1: contact-dependent control of immunity. *Nature reviews. Immunology* **6**, 433-446 (2006). https://doi.org/10.1038/nri1864

22 Zebhauser, R. *et al.* Identification of a novel group of evolutionarily conserved members within the rapidly diverging murine Cea family. *Genomics* **86**, 566-580 (2005). https://doi.org/10.1016/j.ygeno.2005.07.008

23 Chan, C. H. & Stanners, C. P. Novel mouse model for carcinoembryonic antigen-based therapy. *Molecular therapy : the journal of the American Society of Gene Therapy* **9**, 775-785 (2004). https://doi.org/10.1016/j.ymthe.2004.03.009

24 Shifrin, D. A., Jr., Demory Beckler, M., Coffey, R. J. & Tyska, M. J. Extracellular vesicles: communication, coercion, and conditioning. *Mol Biol Cell* **24**, 1253-1259 (2013). https://doi.org/10.1091/mbc.E12-08-0572

25 Cocucci, E. & Meldolesi, J. Ectosomes and exosomes: shedding the confusion between extracellular vesicles. *Trends Cell Biol* **25**, 364-372 (2015). https://doi.org/10.1016/j.tcb.2015.01.004

26 Shifrin, D. A., Jr. *et al.* Enterocyte microvillus-derived vesicles detoxify bacterial products and regulate epithelial-microbial interactions. *Curr Biol* **22**, 627-631 (2012). https://doi.org/10.1016/j.cub.2012.02.022

27 Horstman, A. L. & Kuehn, M. J. Enterotoxigenic Escherichia coli secretes active heat-labile enterotoxin via outer membrane vesicles. *The Journal of biological chemistry* **275**, 12489-12496 (2000). https://doi.org/10.1074/jbc.275.17.12489

28 Roy, K., Hamilton, D. J., Munson, G. P. & Fleckenstein, J. M. Outer Membrane Vesicles Induce Immune Responses to Virulence Proteins and Protect against Colonization by Enterotoxigenic Escherichia coli. *Clinical and vaccine immunology : CVI* **18**, 1803-1808 (2011). https://doi.org/10.1128/CVI.05217-11

29 Kesty, N. C., Mason, K. M., Reedy, M., Miller, S. E. & Kuehn, M. J. Enterotoxigenic Escherichia coli vesicles target toxin delivery into mammalian cells. *EMBO J* **23**, 4538-4549 (2004). https://doi.org/10.1038/sj.emboj.7600471

30 Mayr, B. & Montminy, M. Transcriptional regulation by the phosphorylation-dependent factor CREB. *Nat Rev Mol Cell Biol* **2**, 599-609 (2001).

31 Zhang, X. *et al.* Genome-wide analysis of cAMP-response element binding protein occupancy, phosphorylation, and target gene activation in human tissues. *Proc Natl Acad Sci U S A* **102**, 4459-4464 (2005). https://doi.org/10.1073/pnas.0501076102

32 Sheikh, A. *et al.* Enterotoxigenic Escherichia coli heat-labile toxin drives enteropathic changes in small intestinal epithelia. *Nature communications* **13**, 6886 (2022). https://doi.org/10.1038/s41467-022-34687-7

33 Johansson, M. E., Thomsson, K. A. & Hansson, G. C. Proteomic analyses of the two mucus layers of the colon barrier reveal that their main component, the Muc2 mucin, is strongly bound to the Fcgbp protein. *Journal of proteome research* **8**, 3549-3557 (2009). https://doi.org/10.1021/pr9002504

34 Ehrencrona, E. *et al.* The IgGFc-binding protein FCGBP is secreted with all GDPH sequences cleaved but maintained by interfragment disulfide bonds. *The Journal of biological chemistry* **297**, 100871 (2021). https://doi.org/10.1016/j.jbc.2021.100871

35 Postema, M. M., Grega-Larson, N. E., Neininger, A. C. & Tyska, M. J. IRTKS (BAIAP2L1) Elongates Epithelial Microvilli Using EPS8-Dependent and Independent Mechanisms. *Curr Biol* **28**, 2876-2888 e2874 (2018). https://doi.org/10.1016/j.cub.2018.07.022

36 Gaeta, I. M., Meenderink, L. M., Postema, M. M., Cencer, C. S. & Tyska, M. J. Direct visualization of epithelial microvilli biogenesis. *Curr Biol* **31**, 2561-2575 e2566 (2021). https://doi.org/10.1016/j.cub.2021.04.012

37 Clayton, A., Harris, C. L., Court, J., Mason, M. D. & Morgan, B. P. Antigen-presenting cell exosomes are protected from complement-mediated lysis by expression of CD55 and CD59. *European journal of immunology* **33**, 522-531 (2003). https://doi.org/10.1002/immu.200310028

38 Thery, C., Ostrowski, M. & Segura, E. Membrane vesicles as conveyors of immune responses. *Nature reviews. Immunology* **9**, 581-593 (2009). https://doi.org/10.1038/nri2567

39 McConnell, R. E. *et al.* The enterocyte microvillus is a vesicle-generating organelle. *J Cell Biol* **185**, 1285-1298 (2009). https://doi.org/10.1083/jcb.200902147

40 Matsuoka, Y. *et al.* Immunochemical differences among carcinoembryonic antigen in tumor tissues and related antigens in meconium and adult feces. *Cancer research* **42**, 2012-2018 (1982).

41 Matsuoka, Y. *et al.* Highly effective extraction of carcinoembryonic antigen with phosphatidylinositol-specific phospholipase C. *Tumour Biol* **12**, 91-98 (1991). https://doi.org/10.1159/000217693

42 Kammerer, R. & Zimmermann, W. Coevolution of activating and inhibitory receptors within mammalian carcinoembryonic antigen families. *BMC Biol* **8**, 12 (2010). https://doi.org/10.1186/1741-7007-8-12

43 Baker, E. P. *et al.* Evolution of host-microbe cell adherence by receptor domain shuffling. *Elife* **11** (2022). https://doi.org/10.7554/eLife.73330

44 Zimmermann, W. Evolution: Decoy Receptors as Unique Weapons to Fight Pathogens. *Curr Biol* **29**, R128-R130 (2019). https://doi.org/10.1016/j.cub.2018.12.006

45 Adrian, J., Bonsignore, P., Hammer, S., Frickey, T. & Hauck, C. R. Adaptation to Host-Specific Bacterial Pathogens Drives Rapid Evolution of a Human Innate Immune Receptor. *Curr Biol* **29**, 616-630 e615 (2019). https://doi.org/10.1016/j.cub.2019.01.058

46 Schmitter, T., Agerer, F., Peterson, L., Munzner, P. & Hauck, C. R. Granulocyte CEACAM3 is a phagocytic receptor of the innate immune system that mediates recognition and elimination of human-specific pathogens. *J Exp Med* **199**, 35-46 (2004). https://doi.org/10.1084/jem.20030204

47 Brierley, S. M. Guanylate cyclase-C receptor activation: unexpected biology. *Curr Opin Pharmacol* **12**, 632-640 (2012). https://doi.org/10.1016/j.coph.2012.10.005

48 Cilibrasi, C. *et al.* Definition of an Inflammatory Biomarker Signature in Plasma-Derived Extracellular Vesicles of Glioblastoma Patients. *Biomedicines* **10** (2022). https://doi.org/10.3390/biomedicines10010125

49 Gonzales, P. A. *et al.* Large-scale proteomics and phosphoproteomics of urinary exosomes. *J Am Soc Nephrol* **20**, 363-379 (2009). https://doi.org/10.1681/ASN.2008040406

50 Kobayashi, K., Hamada, Y., Blaser, M. J. & Brown, W. R. The molecular configuration and ultrastructural locations of an IgG Fc binding site in human colonic epithelium. *J Immunol* **146**, 68-74 (1991).

51 Kobayashi, K. *et al.* Distribution and partial characterisation of IgG Fc binding protein in various mucin producing cells and body fluids. *Gut* **51**, 169-176 (2002). https://doi.org/10.1136/gut.51.2.169

52 Harada, N. *et al.* Human IgGFc binding protein (FcgammaBP) in colonic epithelial cells exhibits mucin-like structure. *The Journal of biological chemistry* **272**, 15232-15241 (1997). https://doi.org/10.1074/jbc.272.24.15232

53 Liu, Q. *et al.* Role of the mucin-like glycoprotein FCGBP in mucosal immunity and cancer. *Front Immunol* **13**, 863317 (2022). https://doi.org/10.3389/fimmu.2022.863317

54 Johansson, M. E. *et al.* The inner of the two Muc2 mucin-dependent mucus layers in colon is devoid of bacteria. *Proceedings of the National Academy of Sciences of the United States of America* **105**, 15064-15069 (2008). https://doi.org/10.1073/pnas.0803124105

55 Birchenough, G. M., Johansson, M. E., Gustafsson, J. K., Bergstrom, J. H. & Hansson, G. C. New developments in goblet cell mucus secretion and function. *Mucosal Immunol* **8**, 712-719 (2015). https://doi.org/10.1038/mi.2015.32

56 Nystrom, E. E. L., Arike, L., Ehrencrona, E., Hansson, G. C. & Johansson, M. E. V. Calcium-activated chloride channel regulator 1 (CLCA1) forms non-covalent oligomers in colonic mucus and has mucin 2-processing properties. *The Journal of biological chemistry* **294**, 17075-17089 (2019). https://doi.org/10.1074/jbc.RA119.009940

57 Sheikh, A. *et al.* Enterotoxigenic Escherichia coli Degrades the Host MUC2 Mucin Barrier To Facilitate Critical Pathogen-Enterocyte Interactions in Human Small Intestine. *Infection and immunity* **90**, e0057221 (2022). https://doi.org/10.1128/IAI.00572-21

58 Mercado, E. H. *et al.* Fecal leukocytes in children infected with diarrheagenic Escherichia coli. *J Clin Microbiol* **49**, 1376-1381 (2011). https://doi.org/10.1128/JCM.02199-10

59 Mohamed, J. A. *et al.* A novel single-nucleotide polymorphism in the lactoferrin gene is associated with susceptibility to diarrhea in North American travelers to Mexico. *Clin Infect Dis* **44**, 945-952 (2007). https://doi.org/CID41623 [pii]
10.1086/512199

60 Truett, G. E. *et al.* Preparation of PCR-quality mouse genomic DNA with hot sodium hydroxide and tris (HotSHOT). *Biotechniques* **29**, 52, 54 (2000). https://doi.org/10.2144/00291bm09

61 Allen, K. P., Randolph, M. M. & Fleckenstein, J. M. Importance of heat-labile enterotoxin in colonization of the adult mouse small intestine by human enterotoxigenic Escherichia coli strains. *Infection and immunity* **74**, 869-875 (2006).

62 Zhu, Y. *et al.* Molecular Determinants of Enterotoxigenic Escherichia coli Heat-Stable Toxin Secretion and Delivery. *Infection and immunity* **86** (2018). https://doi.org/10.1128/IAI.00526-18

63 Luo, Q., Vickers, T. J. & Fleckenstein, J. M. Immunogenicity and Protective Efficacy against Enterotoxigenic Escherichia coli Colonization following Intradermal, Sublingual, or Oral Vaccination with EtpA Adhesin. *Clinical and vaccine immunology : CVI* **23**, 628-637 (2016). https://doi.org/10.1128/CVI.00248-16

64 Harro, C. *et al.* Live attenuated enterotoxigenic Escherichia coli (ETEC) vaccine with dmLT adjuvant protects human volunteers against virulent experimental ETEC challenge. *Vaccine* (2019). https://doi.org/10.1016/j.vaccine.2019.02.025

835 ## Figures

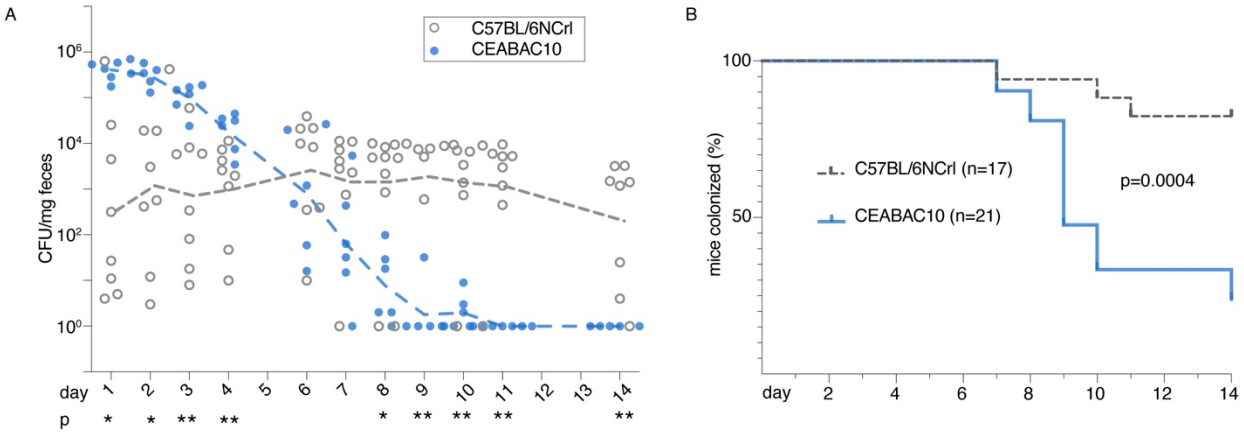

836

837 **figure 1. CEACAM expression alters kinetics of ETEC intestinal colonization A.** ETEC

838 shed in stool following challenge of either C57BL/6NCrl control mice (n=8) or CEABAC10

839 CEACAM-expressing mice (n=6). Dashed lines connect geometric means. *<0.05, **<0.01

840 Mann Whitney two-tailed nonparametric comparison between groups. **B.** Proportion of mice

841 remaining colonized (≥ 1 CFU/mg stool) based on fecal shedding data. Shown are

842 combined results of two independent experiments with total of n=17 control (C57BL/6NCrl)

843 and n=21 CEABAC10 mice. p=0.0004 Log-rank (Mantel-Cox) comparison of survival curves.

844

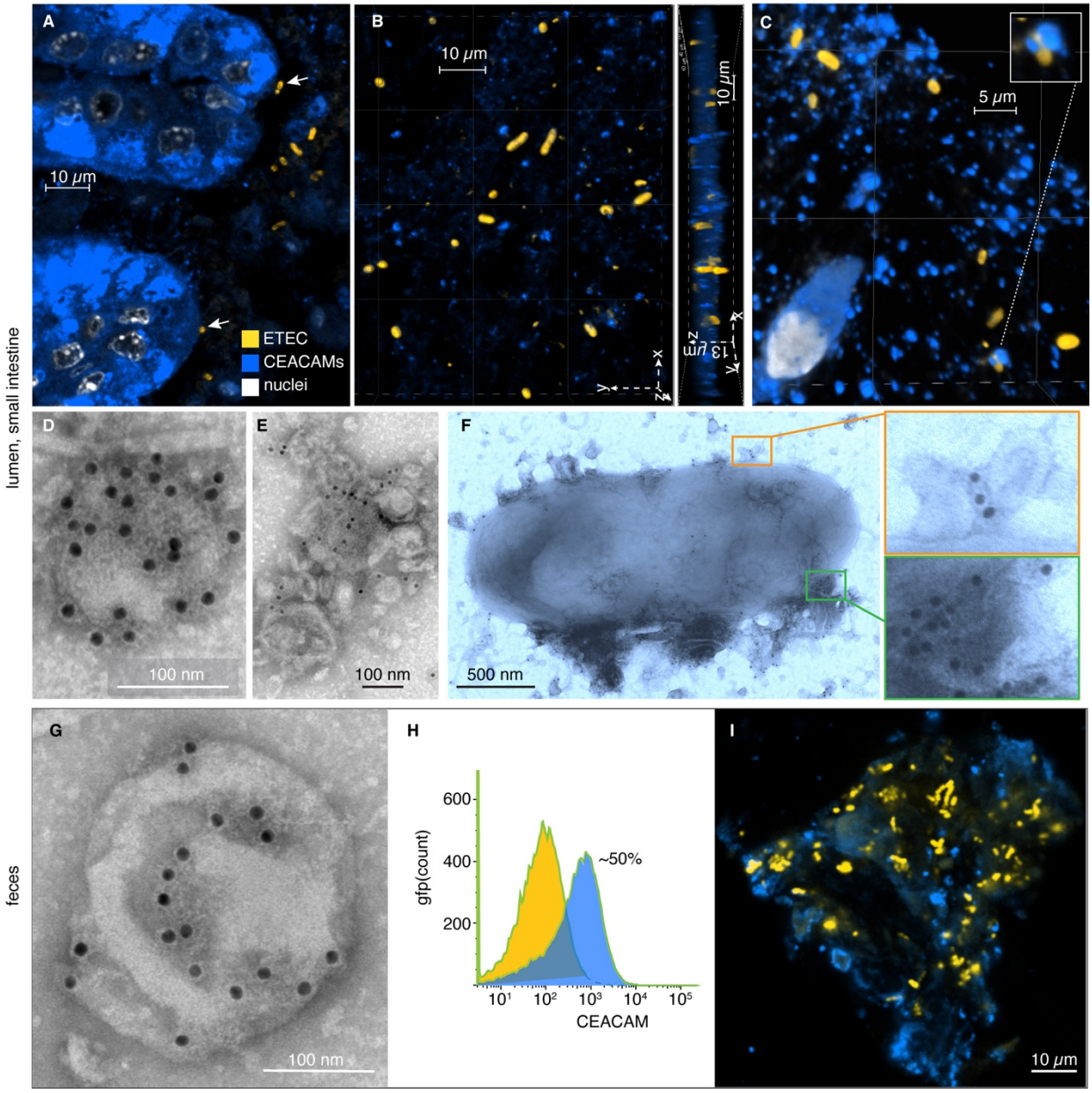

figure 2. ETEC-CEACAM interactions in the intestinal lumen of CEACAM-expressing transgenic mice. Shown are confocal microscopy images of (**A**) ETEC H10407 attached to small intestinal villus enterocytes (arrows) and to CEACAM+ material in the lumen. (**B**). ETEC in the lumen reside in a CEACAM+ matrix. (**C**) Small (~100-300 nm) CEACAM+ structures engage ETEC in the intestinal lumen. Inset shows ETEC surrounded by CEACAM + structures in the lumen. In each panel anti-CEA antibodies were used to identify CEACAMs (blue) and anti-O78 antibodies were used to identify ETEC H10407 (yellow, serotype O78). **D,E**. CEACAM6-positive vesicle, and clusters of EV isolated from ileum of CEABAC10 mouse. **F**. CEACAM6+ EV clustered on the surface of bacteria isolated from ileal lavage following H10407 challenge. **G**. CEACAM6-positive EV isolated from CEABAC10 mouse feces shown by immunogold labeling of anti-CEACAM monoclonal (9A6). **H.** Flow cytometry of GFP+

857 bacteria isolated from fecal resuspension supernatants following challenge of CEABAC10
858 mice with H10407(pGFPmut3.1), showing the proportion of GFP+ bacteria that co-labeled
859 with CEACAMs (blue) vs those which remain unlabeled with CEACAMs (yellow). **I.** Majority of
860 ETEC shed in feces are eliminated in large clusters of CEACAMs. Panel represents individual
861 Z-stack confocal image of fecal resuspension. (GFP+ bacteria pseudo-colored yellow).
862

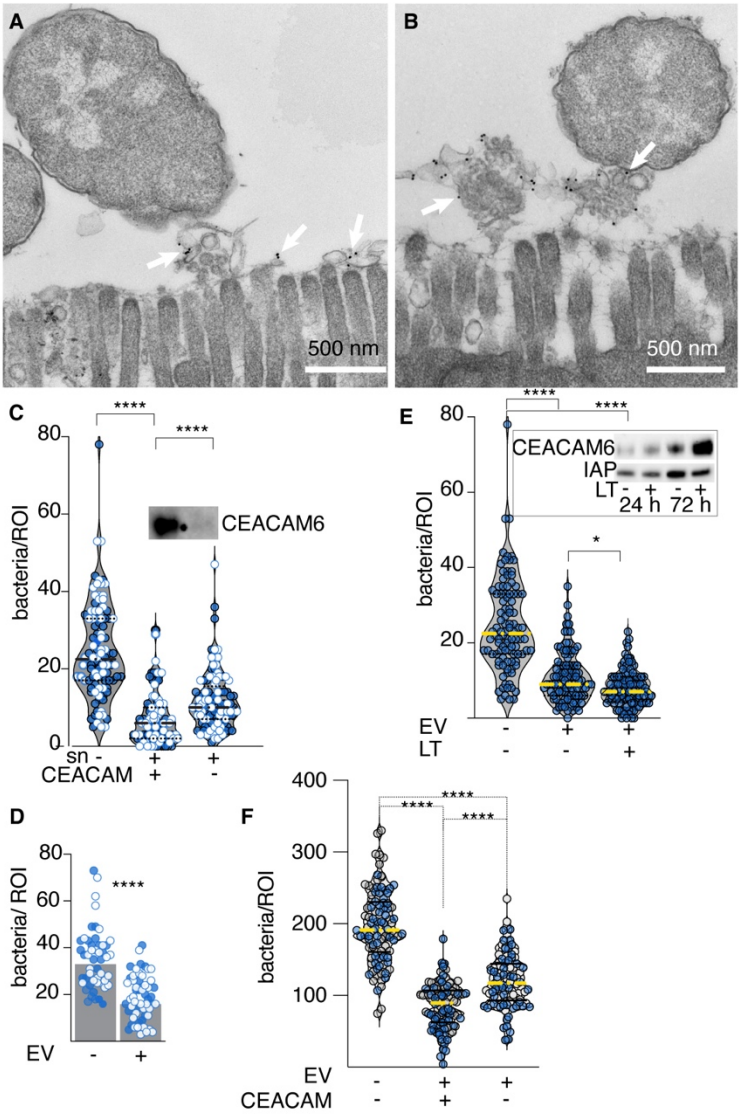

Figure 3 CEACAM-laden EVs block ETEC enterocyte engagement

A. clusters of CEACAM+ extracellular vesicles (EVs) are interposed between the brush border of small intestinal enterocytes and ETEC. **B**. CEACAM+ EVs emerging at the surface of microvilli engage ETEC. (Arrows in A,B indicate immunogold labeling of CEACAM6) **C.** Concentrated supernatants (sn) from polarized small intestinal enteroid monolayers impair ETEC pathogen-host interaction. Columns at left, middle and right of graph indicate no treatment (sn-), treatment with concentrated supernatant (sn+, CEACAM+), and after

872 supernatant absorption of CEACAMs (sn+, CEACAM-). Shown are the results of two
873 independent experiments. ****=p<0.0001 (Kruskall-Wallis). Horizontal lines indicate median
874 and quartiles. Inset immunoblot indicates CEACAM6 before and after absorption. **D.** EVs
875 purified from small intestinal enteroids inhibit attachment of ETEC to target small intestinal
876 epithelia. Shown are the results of 2 replicate experiments. "-"= untreated ileal enteroids
877 (n=50, total); Data reflect bacteria per region of interest (ROI) for wells without (-) and with (+)
878 exogenously added purified EV (n=55 total). ****<0.0001 Mann-Whitney two-tailed
879 nonparametric comparisons. **E**. LT treatment of enteroids enhances CEACAM production on
880 EVs and EV-mediated inhibition of ETEC adhesion to target Caco-2 cells **** <0.0001, *0.02
881 (Kruskal-Wallis). Inset immunoblot shows impact of LT treatment on CEACAM6 expression on
882 EV isolated after treatment for 24, 72 hours. Intestinal alkaline phosphatase (IAP) is shown as
883 a loading control. **F**. EV isolated from murine intestine inhibit ETEC adhesion. Shown are
884 confocal imaging data of ETEC adherent to Caco-2 cells in the absence of EV, EV isolated
885 from CEABAC10 mice (CEACAM+), and parental C57BL6 mice (CEACAM-). ****<0.0001
886 (Kruskal-Wallis). Total of n=100 fields from 2 independent experiments.
887

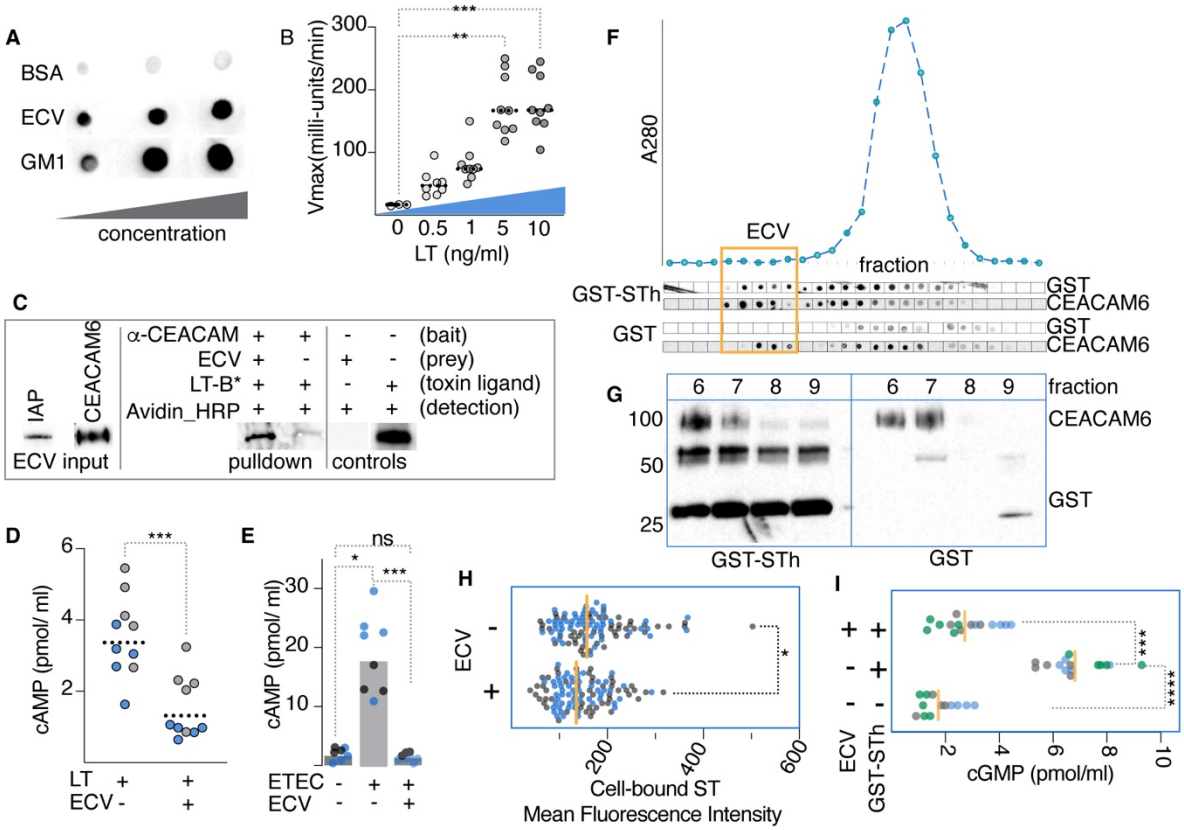

888

889 **figure 4. EV scavenge and neutralize ETEC toxins. A.** EV contain ganglioside receptors for

890 heat-labile toxin (LT). Shown are anti-LT dot immunoblots demonstrating LT-binding to

891 increasing amounts of immobilized BSA (negative control, top) GM-1 ganglioside (positive

892 control, bottom) and EV. **B**. Immobilized EV bind LT. Shown are kinetic ELISA in which EV

893 bound to ELISA plates capture increasing amounts of LT. Summary of three independent

894 experiments, ***0.0008, **0.0014 by Kruskal-Wallis comparisons to no LT control. **C**.

895 Molecular pulldown study using anti-CEACAM antibody coated protein G beads (bait) to pull

896 down EV (prey), and bound heat-labile toxin. Following incubation with biotinylated LT-B (LT-

897 B*), immunoblot was developed with avidin-HRP to detect bound toxin subunit. Immunoblots

898 (left panel) verify presence of intestinal alkaline phosphatase (IAP) and CEACAM6 in EV input

899 prey. Biotinylated LT-B is indicated in blots of pulldown and controls. **D.** EV block LT-

mediated activation of cAMP in target Caco-2 cells. Data reflect baseline-corrected values (raw data-baseline/baseline) and are from two independent experiments (n=10 total replicates). Analysis by Kruskal-Wallis. **E.** EV impede toxin delivery by ETEC. Caco-2 cAMP levels following infection with ETEC H10407 ± EV. Data are from two independent experiments (n=8 total replicates). Analysis by Kruskal-Wallis. **F.** Fractionation of GST-STh/EV complexes by size exclusion chromatography (SEC). Shown below the chromatogram are dot immunoblots for CEACAM6 and GST corresponding to individual fractions. Control fractions from GST-EV interactions are shown below. **G.** Western immunoblot of EV-containing fractions from SEC demonstrating co-elution of CEACAM6 and GST-STh. **H**. EV compete with T84 intestinal epithelial cells for ST binding. Shown are the results of two independent confocal microscopy experiments, with symbols representing mean fluorescence intensity of GST-STh binding in individual fields. Vertical lines represent geometric means. *p=0.02 (Mann-Whitney). **I.** EV neutralize STh activation of cGMP. Shown are results of 3 independent experiments (n=15 technical replicates). ****<0.0001, and ***n=0.0004 by Kruskal-Wallis.

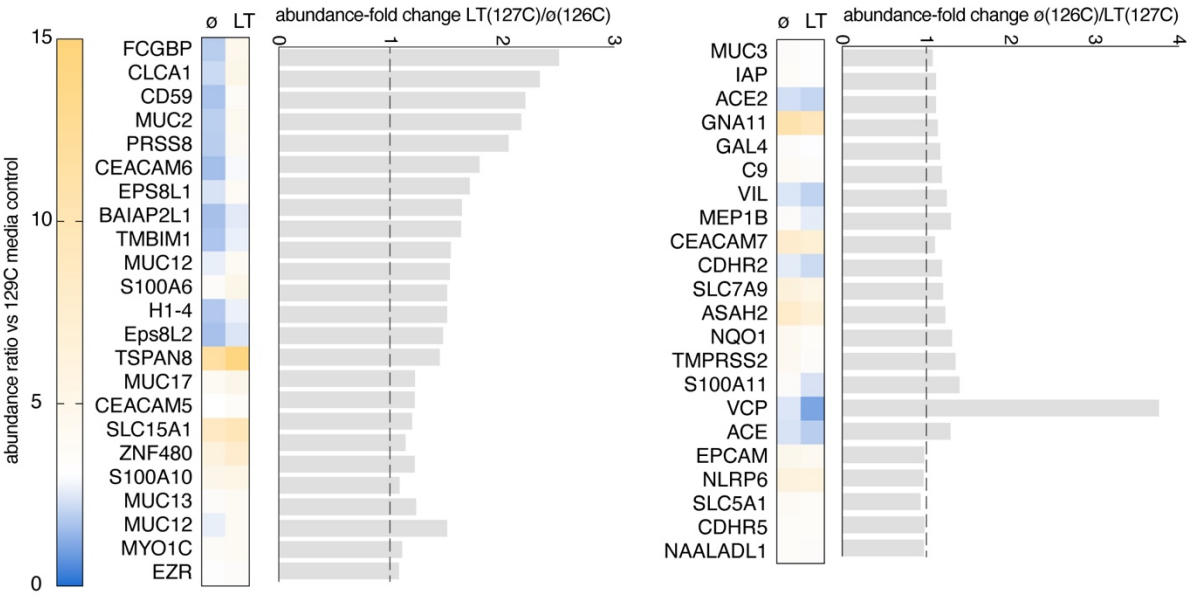

figure 5. Comparative tandem mass tag spectrometry of EVs from LT-treated (127C label) and control (ø, 126C) enteroids. Subset of proteins identified in EVs: which were increased (left) and unchanged or decreased (right) following exposure of enteroids to LT (100 ng/ml overnight ~18 hours).

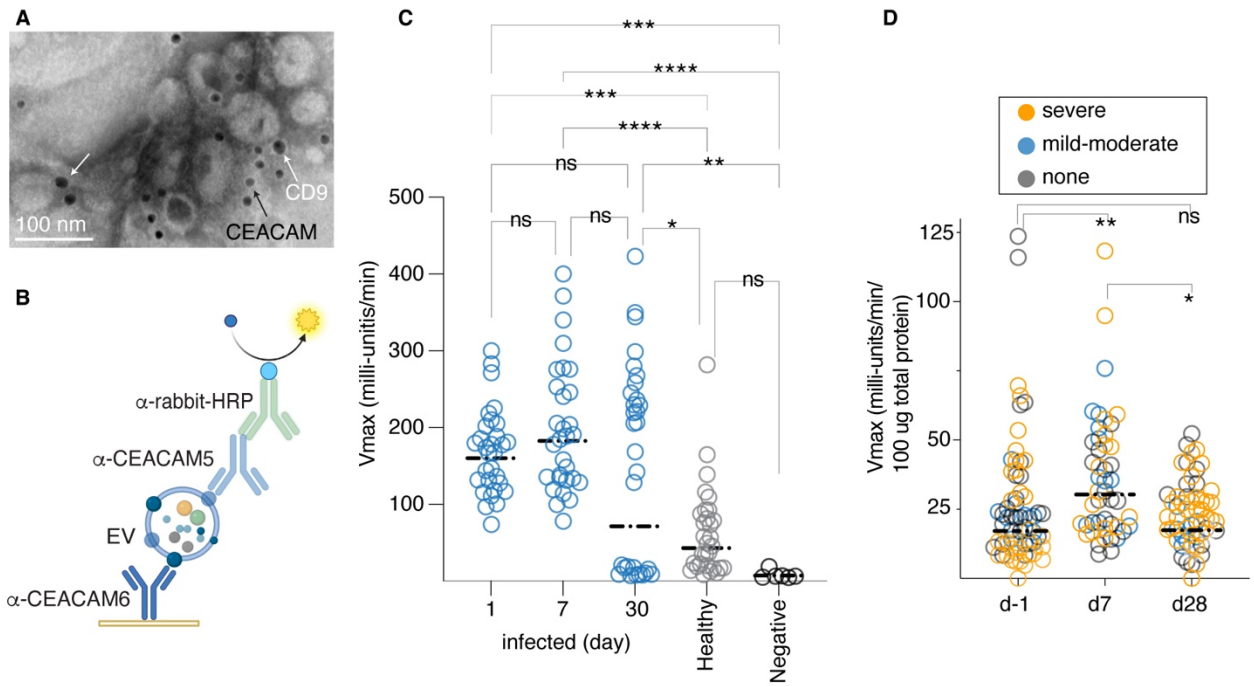

923

924 **Figure 6. human ETEC infection is associated with increases in fecal CEACAMs.**

925 **A**. CEACAM-laden EV are shed in stool of children with acute ETEC diarrheal illness.

926 Immunogold-labeled TEM image of EV isolated from diarrheal stool demonstrates detection

927 of CD9 (larger 18 nm particles, white arrows), and CEACAMs (12 nm, black arrow). **B**.

928 Schematic of kinetic ELISA strategy to capture and detect CEACAM+ EV from human stool.**.**

929 **C**. Graph depicts summary of two independent experiments performed on samples from 5

930 patients naturally-infected with ETEC and 5 healthy controls (icddr,b in Dhaka), each with

931 three technical replicates (total of n=30 data points for each day). Day 1 = day of presentation

932 to icddr,b. Negative control wells contain only buffer used in sample extraction. **D**. Summary

933 of two technical replicates in 2 separate experiments with samples obtained from human

934 volunteers on the day prior to infection (d-1) and on days 7, 28 following challenge with ETEC

935 H10407 (n=17; 3 with mild-moderate diarrhea, 8 with severe diarrhea and 6 with no diarrhea

following challenge). Statistical analyses by Kruskal-Wallis nonparametric comparisons: ****p<0.0001, ***p=0.0002, **p=0.002, *p=0.0127.